Journal of Applied Physics | METHOD | scitation.org/journal/jap

Micro-fabricated caesium vapor cell with 5 mm optical path length

Cite as: J. Appl. Phys. **132**, 204401 (2022); doi: 10.1063/5.0125490
Submitted: 12 September 2022 · Accepted: 4 November 2022 ·
Published Online: 22 November 2022

T. Dyer,[1,a)] S. J. Ingleby,[1] C. Dunare,[2] K. Dodds,[2] P. Lomax,[2] P. F. Griffin,[1] and E. Riis[1]

AFFILIATIONS

[1]Department of Physics, SUPA, University of Strathclyde, Glasgow G4 0NG, United Kingdom
[2]Scottish Microelectronics Centre, University of Edinburgh, Edinburgh EH9 3FF, United Kingdom

[a)]**Author to whom correspondence should be addressed:** terry.dyer@strath.ac.uk

ABSTRACT

Micro-fabricated vapor cells have applications in a number of emerging quantum technology-based devices including miniaturized atomic magnetometers, atomic clocks, and frequency references for laser systems. Increasing the cell optical path length (OPL) and smallest cell dimension are normally desirable to increase the signal to noise ratio (SNR) and minimize the de-polarization rate due to collisions between atomic or molecular species and the cell walls. This paper presents a fully wafer-level scalable fabrication process to manufacture vapor cells with dimensions approaching those of glass-blown cells. The fabrication process is described, and spectroscopic measurements (optical absorption and magnetic resonance) are reported. A magnetic resonance linewidth of 350 Hz is demonstrated, and this is the smallest linewidth reported to date for a micro-fabricated vapor cell.

© 2022 Author(s). All article content, except where otherwise noted, is licensed under a Creative Commons Attribution (CC BY) license (http://creativecommons.org/licenses/by/4.0/). https://doi.org/10.1063/5.0125490

I. INTRODUCTION

One of the major advantages of micro-fabrication for vapor cell production is the ability to process many cells in parallel at the wafer level.[1–3] Leveraging semiconductor industry process control techniques can enable a high yield process resulting in significant economies of scale over glass-blown cells.

Glass-blown vapor cells are traditionally used in high performance atomic clocks, magnetometers, and frequency references.[4,5] The first micro-fabricated vapor cells were developed using anisotropic wet etching of ⟨100⟩ silicon wafers.[6] More advanced techniques, such as deep reactive ion etching (DRIE), allowed the creation of increasingly complex cell geometries including interconnected reservoir/optical probe cells.[7] One downside of this approach is higher unit cost due in part to the reduced number of vapor cells per wafer. Both approaches require photolithography to define vapor cell apertures prior to bulk silicon etching. The OPL of these vapor cells is set by the thickness of the silicon wafer. Unfortunately, thick silicon wafers can be difficult to source, require extended process times, and are often incompatible with the standard semiconductor processing equipment.

One approach[8] to increase the OPL is to build an elongated cell along the silicon wafer surface plane. In our simpler approach, we use a thick BF33 glass wafer to set the OPL with apertures created by water-jet machining (recent work has also used this process to create apertures in a thick silicon wafer[9]). Water-jetting is an attractive method for fabricating vapor cells as the process is low-cost and does not require a clean room; photolithography is not required as the mask design file can be read directly by the water-jet tool.

There is also a vapor cell performance advantage, especially, for battery-operated portable devices. The thermal conductivity of BF33 glass is lower than for silicon, and its specific heat capacity is higher (Table I). Therefore, a vapor cell fabricated principally from BF33 glass will have improved thermal stability over a silicon-based vapor cell.

Low-temperature silicon-glass anodic bonding[11] has dominated the development of micro-fabricated alkali vapor cells. It is used to form both bonds in the conventional glass-silicon-glass wafer stack and results in high hermeticity. Our approach uses a combination of fusion (direct) and anodic bonding to enable bonding of both glass–glass and silicon–glass wafers. Fusion bonding has not previously been reported in vapor cell fabrication, in part, due to the stringent cleanliness and surface property requirements.[12] However, by designing the process flow such that

© Author(s) 2022

TABLE I. Selected thermal properties of silicon and BF33 glass wafers.[10]

	Silicon	BF33 glass
Thermal conductivity W/(m K)	148	1.2
Specific heat capacity J/(kg K)	700	830

fusion bonding occurs at the start of the process, we can subcontract this step to a manufacturer with the necessary clean room infrastructure. This additional capability enables a novel vapor cell architecture with cell dimensions approaching those of glass-blown ones.

Finally, alkali metal can be introduced into the vapor cell using several methods.[13] We have selected aqueous CsN_3 dispense/UV activation[14] as it is low-cost and can be conveniently carried out using precision fluid dispensing robotic systems and 254 nm UV cross-linker exposure tools.

II. VAPOR CELL FABRICATION PROCESS

Micro-fabricated rubidium vapor cells with OPL = 4 mm have been reported previously using mechanical drilling of a glass wafer and a hybrid fabrication process requiring four anodic bonds.[15] Our entirely wafer-level fabrication process (Fig. 1) uses water-jetting to form the glass cavity, extends the OPL to 5 mm, and reduces the number of bonds required to two. Reducing the number of bonds is a key to maintain a low stress wafer stack and enables a full wafer level process. Water jetting also results in smoother sidewalls compared to mechanical drilling. The water-jet process creates apertures in the glass wafer with near vertical sidewalls tapered by 3°–5°. The aperture size tolerance is ±0.1 mm, and the minimum corner radius is ≈0.5 mm. This leads to a preferred circular or rounded square/rectangle aperture suitable for fabricating atomic vapor cells.

Optical access to the vapor cell is via the upper fusion bonded glass window, and light is reflected from the lower anodic bonded Si wafer that contains a patterned dielectric mirror. The external vapor cell BF33 glass sidewall smoothness is determined by the mechanical dicing process and can be controlled to near optical quality. We are investigating about polishing the rougher BF33 glass internal sidewall [Fig. 1(g)], generated by the water-jetting process, to allow light beams to be directed through the vapor cell sidewalls. Our early results demonstrate that this surface can be polished to optical quality in a separate process step prior to fusion bonding.

An example of the level of process control required to ensure high yield is shown in Fig. 2 for the case of anodic bonding. The vapor cell N_2 buffer gas pressure can be set principally through

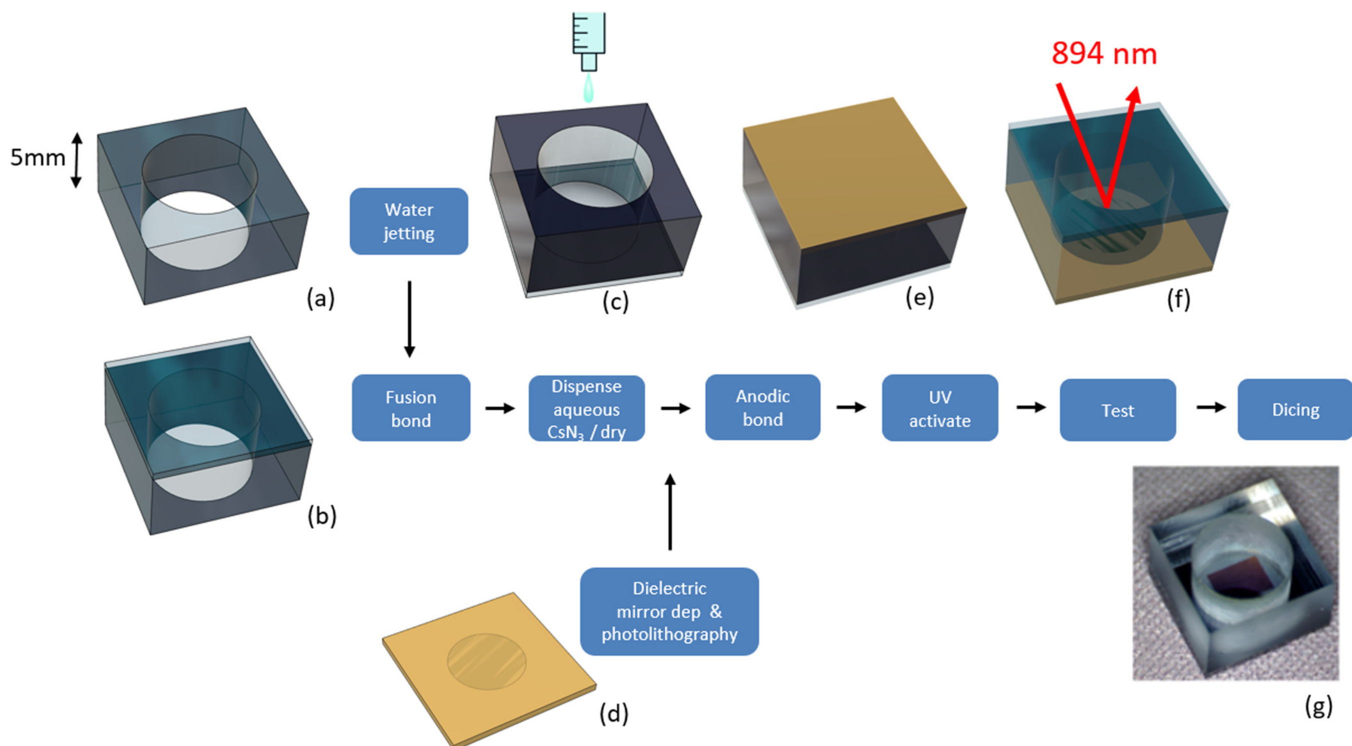

FIG. 1. Cell level illustration of the 150 mm wafer fabrication process (each wafer contains 120 cells). A 5 mm thick BF33 glass wafer is water-jet processed (a). One surface is then fusion bonded (b) to a 0.5 mm BF33 glass wafer. Aqueous CsN_3 is dispensed into the open cavity (c) and dried in a controlled environment. A silicon wafer containing patterned dielectric mirrors (d) is then aligned and anodically bonded to the open glass cavity (e). UV activation of CsN_3 is carried out to generate elemental Cs and N_2. Finally, cells are tested at the wafer level (f) before mechanical dicing (g).

© Author(s) 2022

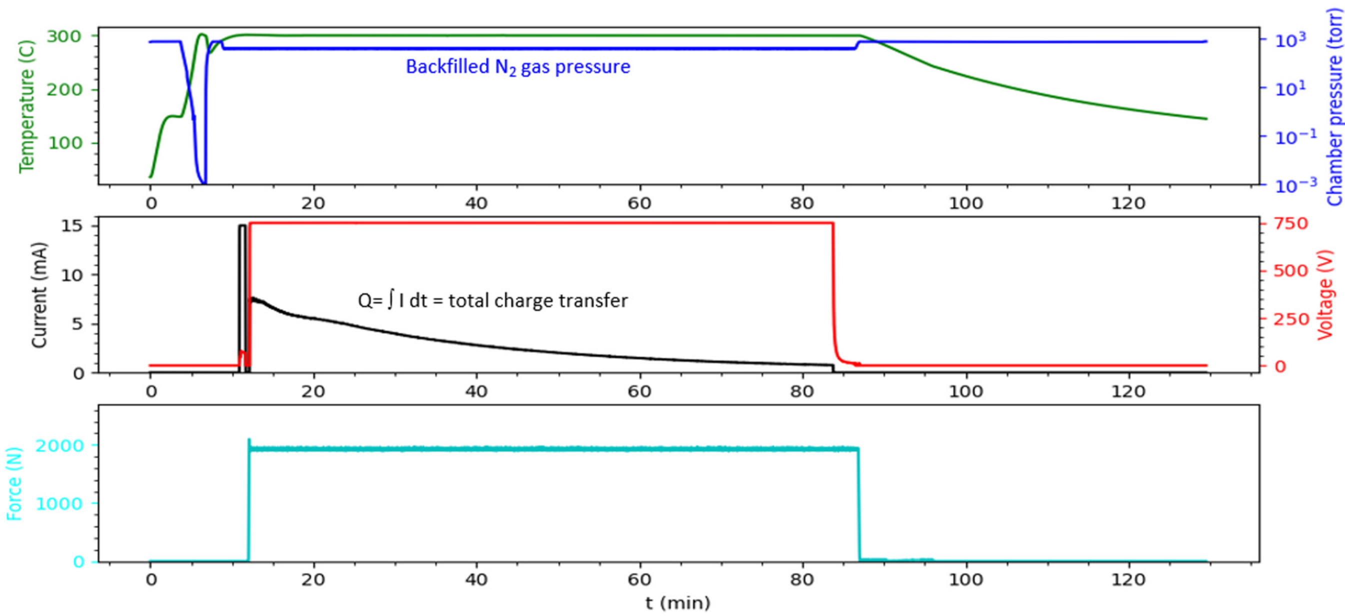

FIG. 2. Example of anodic bonding machine event sequence and process control [step (e) in Fig. 1]. The 3 plots illustrate temperature, pressure, anodic bonding current, and applied force as a function of elapsed process time. The backfilled N_2 pressure is additive to the (≈10x smaller) N_2 pressure generated during the CsN_3 UV activation process. The total charge transfer, Q, is a reliable indicator of the hermeticity of the anodic bond.

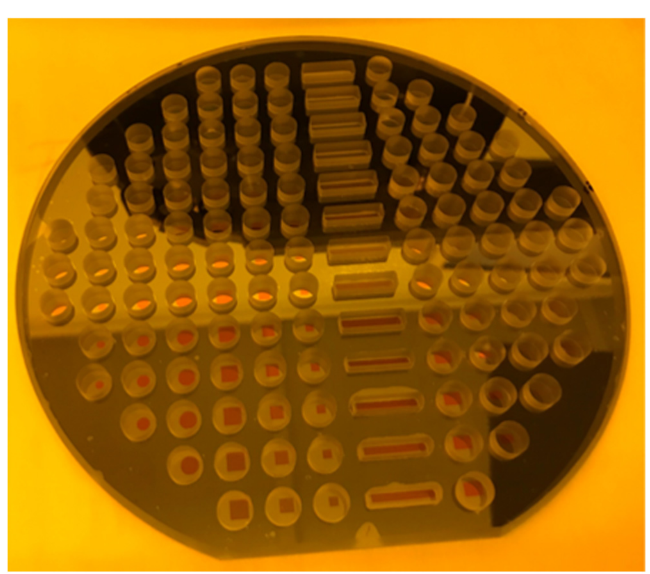

FIG. 3. Fully processed 150 mm wafer stack 6 mm thick containing 120 individual vapor cells with a range of aperture sizes and dielectric mirror configurations. The cell windows are clear of CsN_3 crystal residue.

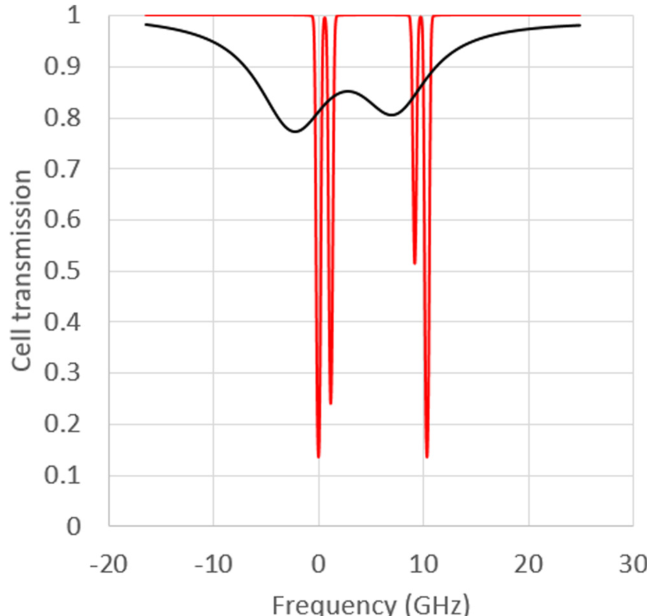

FIG. 4. Fitted transmission spectra for a 5 mm thick micro-fabricated caesium cell (black line) at 85 °C and a caesium reference cell (red line). The frequency axis is scaled relative to the $F_{ground} = 4 \rightarrow F_{excited} = 3$ transition of the caesium D1 line.

© Author(s) 2022

pressure control of the backfilled N_2 introduced into the chamber prior to bringing the two wafers into contact. Due to the safety requirement not to flip the open cavities after CsN_3 dispense [Fig. 1(c)], anodic bonding is carried out with the Si wafer uppermost and biased positively with respect to the grounded glass wafer stack. The molar concentration of CsN_3 = 20 mM in DI water, and the actual dispensed volume/cell depends on the cell volume. One concern with the aqueous CsN_3 dispense/UV activation method is the presence of dried CsN_3 crystals in the optical path of the vapor cell, leading to reduced optical transparency. Through careful control of the evaporation kinetics, we ensure that the dried CsN_3 crystals are located on the inner cell sidewalls [Figs. 1(g) and 3].

III. VAPOR CELL CHARACTERIZATION

A. Optical absorption spectroscopy

Optical absorption spectroscopy is carried out at wafer level to measure pressure broadening due to N_2 buffer gas. The 5 mm micro-fabricated cells are probed by a double pass of a low-intensity linearly polarized light beam. The laser intensity is maintained below the resonant saturation intensity of $I_{sat} = 25\,\mu W\,mm^{-2}$ to avoid power broadening.[16] A reference setup was used to normalize the intensity variation of the laser and to provide a relative and absolute frequency reference.

Figure 4 illustrates the typical spectrum of a 5 mm micro-fabricated cell. The cell spectrum is both broadened and shifted with respect to the caesium reference cell spectrum. A cell pressure of 430 Torr is estimated from a fit to a Voigt profile,[17] and this value is in agreement with the targeted value. At this buffer gas pressure, the four caesium D1 hyperfine transitions cannot be resolved and only two broadened transmission dips are observed.

Our optical absorption spectroscopy setup is coupled to a semi-automated wafer probe station with a heated chuck enabling wafer level cell testing. This approach is borrowed from the semiconductor industry and is a key to enable rapid testing and the "inking out" of cells outside specification that can be later discarded at the dicing stage. Figure 5 shows a wafer map for a fully processed 150 mm wafer. Each cell is labeled with its measured N_2 pressure broadening value. Wafer maps containing other parametric parameters such as absorption, broadening, and shift can be readily generated.

B. Magnetic resonance spectroscopy

5 mm micro-fabricated cells have been successfully integrated into a portable double-resonance atomic magnetometer.[18] This is a single-beam magnetometer, avoiding any requirement for extensive optical hardware or full-field compensation. Magnetic resonance in atomic polarization is detected using a polarimeter to measure optical rotation in transmitted pump light, allowing rejection of common-mode optical noise. We have fabricated wafers containing vapor cells at a range of different buffer gas pressures. Our initial characterization results demonstrate a ground-state Cs spin decay rate of 350 Hz (excluding the effects of magnetic modulation saturation) calculated[19] from a fit to the data in Fig. 6 from a cell with 200 Torr N_2 buffer gas. This represents an ≈3x improvement on the previous work.[3] Future work will include characterization of magnetic resonance linewidth vs buffer gas pressure.

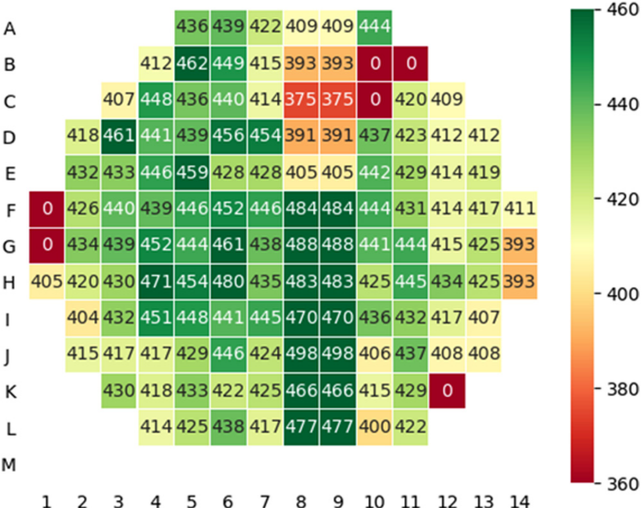

FIG. 5. Wafer map of vapor cell pressure broadening due to N_2 buffer gas across the 150 mm wafer stack in Fig. 3. The functional yield is 95% (cells labelled "0" are defective), and the average cell pressure is 432 Torr with $1\,\sigma = 22$ Torr.

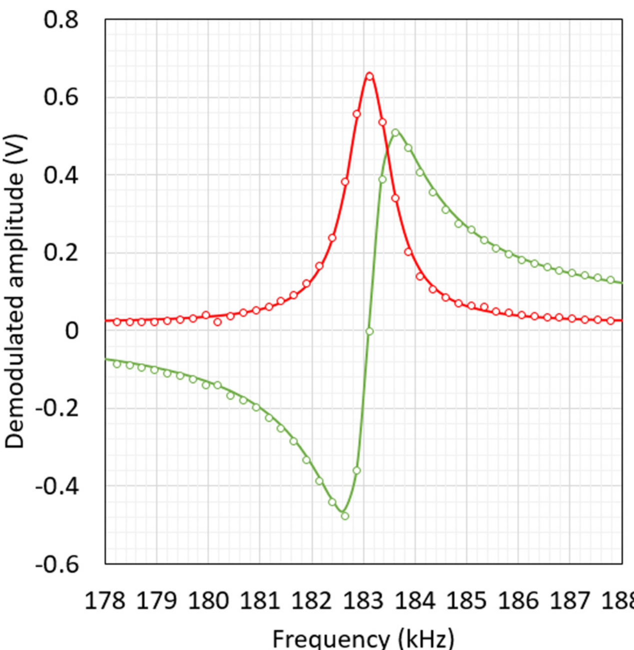

FIG. 6. In-phase and quadrature components of the magnetic resonance signal for an applied RF magnetic field that is swept through the Larmor frequency. The magnetic resonance linewidth is 350 Hz.

© Author(s) 2022

IV. CONCLUSIONS

We have developed a high-yield wafer level process for 5 mm OPL micro-fabricated caesium vapor cells and demonstrated magnetic resonance linewidth of 350 Hz from a cell with 200 Torr N_2 buffer gas, and this is the smallest linewidth reported to date for a micro-fabricated vapor cell. The process can be readily modified at the anodic bonding stage to target an N_2 buffer gas pressure over the range 50 →1500 Torr. Potential future work includes cell aging studies, investigating different buffer gas compositions, alkali metals, and the development of a fully fusion bonded micro-fabricated atomic vapor cell.

ACKNOWLEDGMENTS

The authors would like to thank Dr. Jonathan Pritchard for his work on the optical absorption spectroscopy setup. This work was funded in part by the UK Quantum Technology Hub in Sensing and Timing, EPSRC (Grant No EP/T001046/1).

AUTHOR DECLARATIONS

Conflict of Interest

The authors have no conflicts to disclose.

Author Contributions

T. Dyer: Conceptualization (lead); Data curation (equal); Formal analysis (lead); Investigation (equal); Methodology (equal); Visualization (lead); Writing – original draft (lead); Writing – review & editing (lead). **S. J. Ingleby:** Data curation (equal); Investigation (equal); Validation (equal); Writing – review & editing (supporting). **C. Dunare:** Investigation (equal); Methodology (equal); Validation (equal). **K. Dodds:** Investigation (equal); Methodology (equal); Validation (equal). **P. Lomax:** Investigation (equal); Methodology (equal); Project administration (equal); Resources (equal); Supervision (equal); Writing – review & editing (supporting). **P. F. Griffin:** Funding acquisition (equal); Project administration (equal); Resources (equal); Supervision (equal); Writing – review & editing (supporting). **E. Riis:** Conceptualization (equal); Funding acquisition (equal); Project administration (equal); Resources (equal); Supervision (lead); Writing – original draft (supporting); Writing – review & editing (supporting).

DATA AVAILABILITY

The data that support the findings of this study are openly available in the University of Strathclyde KnowledgeBase at https://doi.org/10.15129/3ce0aa0f-7561-4997-a867-a89d6accf18c, Ref. [20].

REFERENCES

[1] T. Overstolz, J. Haesler, and V. Spassov, U.S. patent 8,906,470 B2 (9 December 2014).

[2] R. Vicarini, V. Maurice, M. Hafiz, J. Rutkowski, C. Gorecki, N. Passilly, L. Ribetto, V. Gaff, V. Volant, S. Galliou, and R. Boudot, "Demonstration of the mass-producible feature of a Cs vapor microcell technology for miniature atomic clocks," Sens. Actuator A **280**, 99 (2018).

[3] R. Zhang, T. Dyer, N. Brockie, R. Parsa, and R. Mhaskar, "Subpicotesla scalar atomic magnetometer with a microfabricated cell," J. Appl. Phys. **126**, 124503 (2019).

[4] J. C. Allred, R. N. Lyman, T. Kornack, and M. Romalis, "High-sensitivity atomic magnetometer unaffected by spin-exchange relaxation," Phys. Rev. Lett. **89**, 130801 (2002).

[5] E. J. Eklund, A. M. Shkel, S. Knappe, E. Donley, and J. Kitching, "Glass-blown spherical microcells for chip-scale atomic devices," Sens. Actuator A **143**, 175 (2008).

[6] L.-A. Liew, S. Knappe, J. Morland, H. Robinson, L. Hollberg, and J. Kitching, "Microfabricated alkali atom vapor cells," Appl. Phys. Lett. **84**, 2694 (2004).

[7] B. Bopp, V. Maurice, and J. Kitching, "Wafer-level fabrication of alkali vapor cells using in-situ atomic deposition atom vapor cells," J. Phys. Photonics **3**, 015002 (2021).

[8] R. Chutani, V. Maurice, N. Passilly, C. Gorecki, R. Boudot, M. A. Hafiz, P. Abbé, S. Galliou, J.-Y. Rauch, and E. de Clercq, "Laser light routing in an elongated micromachined vapor cell with diffraction gratings for atomic clock applications," Sci. Rep. **5**, 14001 (2015).

[9] S. Dyer, P. F. Griffin, A. S. Arnold, F. Mirando, D. P. Burt, E. Riis, and J. P. McGilligan, "Micro-machined deep silicon atomic vapor cells," J. Appl. Phys. **132**, 134401 (2022).

[10] D. Xia, L. Huang, L. Xu, and H. Gao, "Structural analysis of disk resonance gyroscope," Micromachines **8**, 296 (2017).

[11] K. Malecki and F. G. D. Corte, "Silicon-glass anodic bonding at low temperature," Proc. SPIE **5715**, 180 (2005).

[12] A. Plößl and G. Kräuter, "Wafer direct bonding: Tailoring adhesion between brittle materials," Mat. Sci. Eng.: R **25**, 1 (1999).

[13] P. Knapkiewicz, "Technological assessment of MEMS alkali vapor cells for atomic references," Micromachines **10**, 25 (2018).

[14] S. Woetzel, V. Schultze, R. IJsselsteijn, T. Schulz, S. Anders, R. Stolz, and H.-G. Meyer, "Microfabricated atomic vapor cell arrays for magnetic field measurements," Rev. Sci. Instrum. **82**, 033111 (2011).

[15] Y. Pétremand, C. Affolderbach, R. Straessle, M. Pellaton, D. Briand, G. Mileti, and N. F. de Rooij, "Microfabricated rubidium vapour cell with a thick glass core for small-scale atomic clock applications," J. Micromech. Microeng. **22**, 025013 (2012).

[16] D. Hunter, "Chip-scale atomic magnetometer based on free-induction-decay," Ph.D. thesis (University of Strathclyde, 2019).

[17] G. A. Pitz, D. E. Wertepny, and G. P. Perram, "Pressure broadening and shift of the cesium D_1 transition by the noble gases and N_2, H_2, HD, D_2, CH_4, C_2H_6, CF_4, and ^3He," Phys. Rev. A **80**, 062718 (2009).

[18] S. Ingleby, P. Griffin, T. Dyer, M. Mrozowski, and E. Riis, "A digital alkali spin maser," Sci. Rep. **12**, 12888 (2022).

[19] C. O'Dwyer, S. J. Ingleby, I. C. Chalmers, P. F. Griffin, and E. Riis, "A feed-forward measurement scheme for periodic noise suppression in atomic magnetometry," Rev. Sci. Instrum. **91**, 045103 (2020).

[20] T. Dyer, "Data for: 'Micro-fabricated caesium vapour cell with 5mm optical path length,'" University of Strathclyde, (2020) dataset. https://doi.org/10.15129/3ce0aa0f-7561-4997-a867-a89d6accf18c.

© Author(s) 2022